Article

Direct Ink Writing of Biocompatible Nanocellulose and Chitosan Hydrogels for Implant Mesh Matrices

Rubina Ajdary, Guillermo Reyes, Jani Kuula, Eija Raussi-Lehto, Tomi S. Mikkola, Esko Kankuri, and Orlando J. Rojas*

Cite This: ACS Polym. Au 2022, 2, 97−107

Read Online

ACCESS | Metrics & More | Article Recommendations | Supporting Information

ABSTRACT: Direct ink writing via single or multihead extrusion is used to synthesize layer-by-layer (LbL) meshes comprising renewable polysaccharides. The best mechanical performance (683 ± 63 MPa modulus and 2.5 ± 0.4 MPa tensile strength) is observed for 3D printed structures with full infill density, given the role of electrostatic complexation between the oppositely charged components (chitosan and cellulose nanofibrils). The LbL structures develop an unexpectedly high wet stability that undergoes gradual weight loss at neutral and slightly acidic pH. The excellent biocompatibility and noncytotoxicity toward human monocyte/macrophages and controllable shrinkage upon solvent exchange make the cellular meshes appropriate for use as biomedical implants.

KEYWORDS: Nanocellulose, Chitosan, Layer-by-layer meshes, Medical implants, Direct ink writing
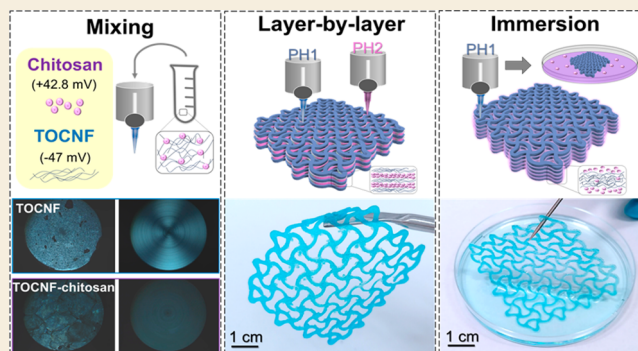
1. INTRODUCTION

Synthetic plastic meshes are commonly used as implants to treat hernia and gynecological pelvic disorders in clinical practice. The implanted mesh supports to lift and holds any weakened tissue in the desired position. Despite the promising mechanical performance of synthetic meshes, which also display up to 82% anatomic success rates, several short and long-term challenges have emerged.[1] For instance, following mesh implant surgery, patients commonly experience adverse symptoms such as pain, internal inflammation, local infection, and implant migration. Most of these issues are associated with the implant mesh material, which does not meet critical structural demands and collapses under the load of the weakened tissue.[2] As a result, the vast majority of hernia meshes are marketed as implants to treat pelvic organ prolapse, which is unfortunate, given that the stress levels are considerably different in these two anatomical cases.[3] Most available mesh implants are made of polypropylene (PP), the same polymer used in indoor and outdoor carpeting. Although PP is inert and resists hydrolytic degradation, recent evidence suggests that PP undergoes dramatic mechanical and chemical changes after implantation. A study with 164 explanted PP meshes demonstrated surface degradation and microcracks in 162 (99%) of the samples.[4] This structural downgrade due to the biochemical environment in the human body (37 °C at given oxygen levels and wide range of pH and salt concentrations) causes superficial inflamed cells and entrapment in the microcracks of the eroded mesh. The adverse associations and patient-reported complications were reasons for the U.S. Food and Drug Administration to ban various PP mesh products available in the market in 2019.[5]

Contrary to plastics, biosourced nanomaterials, such as fibrillated cellulose, have shown promising properties, with no concerns arising from associated sustainable technologies.[6] Nanocellulose has emerged as an auspicious material in biomedicine due to its resemblance to the extracellular matrix (ECM),[7] not to mention its biocompatibility and tunable assembly into geometries with tailorable structural properties.[8] Aqueous suspension of nanocellulose is shear-thinning and allow the fabrication of one-dimensional filaments (via wet-spinning),[9] two-dimensional films (casting and electrospun webs),[10] and three-dimensional layer-by-layer assemblies following additive manufacturing.[8,11] Chitosan, another naturally derived biopolymer produced from the deacetylation of chitin, supports biological and antimicrobial activities. As a positively charged polymer, chitosan contains primary amino groups that are protonated when placed in mild acidic media.[12,13] Although chitosan features excellent biocompatibility and negligible toxicity, it is mainly used as an additive

combined with other polymers due to its insufficient mechanical strength.[14]

Advanced implants engineered using 3D printing and layer-by-layer assembly offer possibilities for individual customization based on the needs of the patient and repair extent. Due to its vast potential for adjusting the critical structural aspects in biomedical implants, the extrusion-based Direct Ink Writing (DIW) technique has emerged as a promising approach. For instance, typical polymeric mesh structures containing small openings (less than 1 mm) yield insufficient tissue integration, enforce inflammation, and enhance bridging fibrosis.[15] With DIW, however, all the required geometrical details such as mesh shape, dimensions, infill density, and opening size can be customized. Hence, nanocellulose-based 3D printed meshes can help to overcome the inherent disadvantages of knitted PP meshes, such as unraveling the structure under load, erosion of heat-sealed parts, or mechanically cutting edges.[16]

Several recent reports have investigated the potential of nanocellulose-based inks for 3D printed patch applications. Olmos-Juste et al.[17] explored curcumin-loaded formulations produced by DIW based on nanocellulose and alginate for local drug administration. We recently reported on drug-loaded, conductive, elastic cardiac patches based on nanocellulose suitable for long-term therapies after myocardial infarction.[18]

Previous studies focused on chitosan are limited to about 1% of the research in 3D printing and about 4% in bioprinting technologies.[19] Most of the 3D printed chitosan systems demonstrated so far indicate poor stability and mechanical performance. Some efforts have addressed the issue by dissolution chitosan into an aqueous alkali solution at low temperatures.[14] The self-assembly of chitosan at high temperatures leads to gelation and promotes inks with shear-thinning behaviors. The development of hydrogel composites is another way to address the challenges associated with the chitosan's weak mechanical properties. In a recent study, a low viscosity chitosan solution (2.0−3.0 wt %) and nanocellulose suspension (0.4 wt %) were printed in an alkali coagulation bath, in the form of filaments and multilayer scaffolds. The results supported the hypothesis that chitosan and nanocellulose biohydrogels are excellent candidates to engineer mechanically demanding soft tissues (e.g., cartilage, intervertebral disc, and meniscus).[20] Chitosan has been mixed with materials such as nanocellulose,[21,22] guar gum,[23] poly(vinyl alcohol),[24] and carbon nanotubes,[25] for instance, to fabricate films and aerogels. However, obtaining high fidelity 3D printed structures with chitosan remains challenging.

This work relies on the electrostatic interactions that arise from the layer-by-layer assembly of anionic (2,2,6,6-tetramethylpiperidin-1-yl)oxidanyl (TEMPO)-oxidized cellulose nanofibrils (TOCNF) and positively charged chitosan, e.g., to retain both materials' outstanding inherent properties while addressing the low mechanical strength of chitosan.

In earlier studies, we investigated the potential of nanocellulose for 3D printed biomedicine as cell culturing scaffolds, cardiac patches, and drug carriers.[18,26] Herein, we propose a 3D printed, nanocellulose/chitosan structure substitute for synthetic meshes. More specifically, the oppositely charged components are 3D printed by either one or multiple printheads, taking advantage of their electrostatic interactions and leading to stable supramolecular interfibrillar structures with enhanced mechanical performance. We explore these 3D printed biomeshes for their microstructure, shrinkage, mechanical, swelling, degradation, cytotoxicity, and proinflammatory cell properties.

2. EXPERIMENTAL SECTION

2.1. Materials

Medium molecular weight chitosan (75−85% acetylation degree), sodium bromide, sodium hypochlorite, and sodium hydroxide were purchased from Sigma-Aldrich. Acetic acid (glacial ≥ 99.7%) was obtained from J.T. Baker, and glutaraldehyde (25%) was purchased from Thermo Fisher Scientific. Phosphate buffer saline (pH 7.4) and acetate buffer solution (pH 5) were used in the characterizations. In addition, Milli-Q water was purified by using a Millipore Synergy UV unit (18.2 MΩ cm) and utilized throughout the experiments. Other solvents include acetone (AnalaR NORMAPUR 99.8%, VWR Chemicals) and ethanol (ETAX Aa 99.5%, Aldrich, Steinheim, Germany). GYNECARE TVT EXACT polypropylene mesh from Johnson & Johnson (New Brunswick, NJ, USA) was used as a control sample in the in vitro test. The THP-1 human monocyte/macrophage cell line was obtained from the European Collection of Authenticated Cell Cultures (ECACC, cat#88081201, Salisbury, UK).

2.2. Design and Fabrication of 3D Printed Meshes Based on Nanocellulose and Chitosan

2.2.1. Preparation of 3D Printing Biomaterial Inks. TEMPO-oxidized cellulose nanofibrils (TOCNF) were produced by TEMPO-mediated oxidation (2,2,6,6-tetramethylpiperidine-1-oxyl) followed by disintegration of never-dried, fines-free, and fully bleached hardwood (birch) fibers collected from a Finnish pulp mill, as described previously.[18,26] Shortly, the cellulose fibers were immersed in Milli-Q water while 0.013 mmol/g TEMPO and 0.13 mmol/g sodium bromide were added to the container. Then, 5 mmol/g sodium hypochlorite was added to the suspension, and the pH was adjusted to 10 by the addition of 0.1 M sodium hydroxide. The mixture was maintained at room temperature and stirred for about 6 h. Then the resulted fibers were washed several times with deionized water until a neutral pH was obtained. Furthermore, the fibers were fibrillated following one pass at a pressure of 1400 bar by a microfluidizer (M-110P, Microfluidics Inc., Newton, MA). The viscous hydrogel was concentrated to 2 wt % by water evaporation on a hot plate under stirring. The 2 wt % chitosan solution was prepared by dissolution of chitosan in 1 vol % acetic acid solution at 50−55 °C.[27] The chitosan was added in several steps and in small amounts to ensure proper polymer dissolution. Then, the closed container was placed in a sonication bath at 50 °C for 30 min to remove bubbles and dissolve the remaining chitosan particles.

2.2.2. Direct Ink Writing of 3D Printed Meshes Based on Nanocellulose and Chitosan. A BIOX bioprinter from CELLINK (Sweden) equipped with pneumatic multi-printheads was utilized to 3D print mesh structures. Mesh structures based on TOCNF and chitosan were developed following three approaches. In the first approach, the TOCNF (2 wt %) and chitosan (2 wt %) were appropriately mixed in an equal mass ratio and placed in a clear pneumatic syringe before printing. In the second approach, 2 wt % TOCNF and 2 wt % chitosan were placed in separate 3 mL clear pneumatic syringes and extruded through 22 gauge (410 μm diameter) and 20 gauge (630 μm diameter) sterile blunt needles, respectively. In this approach, a multilayer mesh structure was developed composed of five layers (three layers of TOCNF and two layers of chitosan). In the third and final approach, the five-layer mesh structure was entirely 3D printed by TOCNF. After printing, the TOCNF mesh was immersed in chitosan 2 wt % to obtain the chitosan sorbed TOCNF mesh. All mesh structures were printed on glass Petri dishes (100 mm diameter). The 3D printed meshes were placed in a freezer overnight after the printing/washing step by DI water. Then, frozen meshes were placed in ethanol following three cycles of solvent exchange to replace the water in the structure. The meshes were retained in ethanol until further use, and some samples were freeze-dried for characterization that required dry samples.

As an additional treatment, the chitosan-sorbed TOCNF was cross-linked by glutaraldehyde treatment to enhance the flexibility of the mesh. The cross-linking was performed by immersing the mesh in 100 mL of glutaraldehyde 5 wt % solution containing 20 μL of hydrochloric acid (1 M) at room temperature as acid catalysis.[28] After 1 h of immersion, the mesh was rinsed with DI water several times. Then, the structure was frozen overnight at −18 °C followed by freeze-drying under vacuum with a FreeZone 2.5 L Benchtop Freeze-Dryer for 48 h at −49 °C.

2.3. Characterization of Inks and 3D Printed Meshes Based on Nanocellulose and Chitosan

2.3.1. Rheology.
The shear rheology of the gel samples was monitored in the steady and oscillatory modes using an Anton Paar Physica MCR 302 (Anton Paar GmbH, Austria) rheometer equipped with a Peltier hood H-PTD 200 for controlled temperature and humidity and a light source with a cross polarizer to allow us to monitor dope birefringence phenomena during the test. The tests were carried out with a parallel plate geometry of 25 mm diameter and 1 mm gap.

2.3.2. Filaments Mechanical Properties.
TOCNF and TOCNF-chitosan gel solutions were stored in 50 mL Luer lock syringe to be extruded using a dispensing needle (Ramé-Hart Instrument CO, outer needle gauge 13 with diameter Φ_i = 1800 μm, and inner needle gauge 21 with inner diameter Φ_o = 508 μm). The wet spinning system uses two pumps (CHEMYX, model NEXUS 6000, and CHEMYX, model FUSION 6000, USA) to extrude the dope into an acid bath (0,001 M HCl) at a volumetric speed of Q = 0.1 mL/min. The filaments' mechanical properties were studied using a Universal Tensile Tester Instron 4204, 1 kN load cell, test speed 10 mm/min. Samples were prepared and analyzed according to the ASTM D3822/D3822 M standard. The samples were stored for 48 h at 50% relative humidity (RH) and 23 °C before each test. For the tests, 40 mm long filaments were cut and fixed to the Instron clamps using sandpaper. The thickness of dry and wet samples (immersed in deionized water overnight) was measured using a digital micrometer (Mitutoyo, Japan) and repeated five times in different positions. Ten replicas of each sample were taken for the mechanical tests.

2.3.3. Zeta Potential.
To access the surface charge of polymers, suspensions at a concentration of 0.1 wt % in 5×10^{-3} M sodium chloride (NaCl) were utilized to measure the ζ-potential at neutral pH by a dip cell on a Malvern, Zetasizer ZS.

2.3.4. Microstructure.
The microstructures of 3D printed mesh were investigated after freeze-drying by a scanning electron microscope (SEM, Zeiss Sigma VP, German). The microscope operated under vacuum and at an accelerated voltage of 2−3 kV. Before the experiment, a piece of the dry samples was fixed on the metal stub using a double-sided carbon tape and coated with a 4−5 nm layer of gold−palladium alloy using a LECIA EM ACE600 sputter coater.

2.3.5. Shrinkage and Infill Density.
The Java-based image processing software, ImageJ,[29] was used to analyze the mesh images at different stages to determine the openings' size, mesh infill density, and shrinkage.

2.3.6. Mechanical Properties.
To measure the mechanical strength, structures were 3D printed with 100% infill density and a gauge length of 50 mm according to ASTM D638 standard. Before the tests, the test specimens were equilibrated for at least 24 h in a room kept at a constant temperature of 23 °C and 50% RH. The tensile properties of the 3D printed samples were tested with a Universal Instron 4240 testing machine using a 100 N load and equipped with an infrared camera with the test speed adjusted to 3 mm min^{-1}. The dry dog-bone specimen was clamped to characterize the samples in the wet condition, and the middle section of the sample was entirely soaked by pipetting deionized water. The measurement was performed after 60 s of wetting the pieces. A minimum of 5 (and a maximum of 10) replicates were measured for the mechanical properties.

2.3.7. Swelling and Weight Loss.
The freeze-dried 3D printed sample was cut into pieces of similar size (by an 8 mm round biopsy punch), and the initial dry weight of the sample was recorded as m_0.

Then the samples were soaked in phosphate buffer solution (pH 7.4) and acetate buffer solution (pH 5) at room temperature, and the samples were taken out at specific time points (day 1, 7, 14, 21, 28). The weight of the piece after each immersion time point was recorded as m_s. The swelling of the samples was calculated using eq 1. Each measurement was repeated five times, and the mean value ± error of the mean was reported.

$$\text{swelling (g/g)} = \frac{m_s - m_0}{m_0} \tag{1}$$

To measure the weight loss at each time point (day 1, 7, 14, 21, 28), the initial weight of the sample after freeze-drying was marked as w_0. Then, the samples were immersed in 10 mL of phosphate buffer solution (pH 7.4) and acetate buffer solution pH 5 at 37 °C. At each time point, the pieces were removed from the buffer, redried at 37 °C for 24 h, and weighed again in the dry state (w_d). Finally, the weight loss was calculated using eq 2.

$$\text{weight loss (\%)} = \frac{W_0 - W_d}{W_0} \times 100 \tag{2}$$

2.3.8. Measurements of Cytotoxicity and Proinflammatory Cell Activation.
THP-1 cells were cultured in Roswell Park Memorial Institute (RPMI)-1640 medium (Gibco 31870-025, Thermo Fisher Scientific, Waltham, MA, USA) supplemented with 10% heat-inactivated fetal bovine serum (Gibco 10500-064), 2 mM L-glutamine (Gibco A2916801), and antibiotics (Gibco 15140-122, penicillin G 100 U/ml, streptomycin 100 μg/mL and Gibco 15290-026, amphotericin B 250 ng/mL) in a humidified atmosphere at +37 °C supplemented with 5% CO$_2$. Coincubation with materials was carried out in wells of a 96-well plate. Replicate samples of materials were cut using a 6 mm diameter biopsy punch (BP-60F, kai Europe GmbH, Solingen, Germany), incubated overnight in 70% ethanol followed by washes in calcium- and magnesium-free phosphate-buffered saline (Lonza Bio Whittaker, 17-516F, Basel, Switzerland). Before each experiment, the materials were incubated overnight in a culture medium. Cells were counted (Countess II, Applied Biosystems, Thermo Fisher Scientific), and 80 000 cells/well were added to each well with the material and the empty control wells without material. 12-O-Tetradecanoylphorbol 13-acetate (TPA, Sigma P8139, Merck KGaA, Darmstadt, Germany) at a final concentration of 300 nM was used to induce macrophage differentiation of the THP-1 cells as reported previously.[30] After a 3 day incubation, the culture medium was collected for analysis. Samples were centrifuged at 20 000 rpm for 10 min, and supernatants were divided into aliquots and then transferred to new tubes for storage at −20 °C until analysis. According to the manufacturer's instructions, cytotoxicity was measured from the culture medium supernatants using the colorimetric LDH cytotoxicity detection kit plus (Roche 04744926001, Merck) and as described earlier.[31] Briefly, 100 μL of the assay reagent was mixed with 100 μL of the cell culture sample supernatant. After a 30 min incubation in the dark at room temperature, the reaction was stopped, and spectrophotometric analysis was performed using a microplate reader. Optical density results at 492 nm were corrected with those at 620 nm. Levels of basal LDH activity measured from naive culture medium samples were subtracted from the obtained values before analysis.

Concentrations of interleukin-8 (IL-8) in the culture medium sample supernatants were measured using a human IL-8 specific enzyme-linked immunosorbent assay quantitative (ELISA, 88-8086; Invitrogen, Thermo Fisher Scientific) according to the manufacturer's instructions. If needed at reanalysis, samples initially measuring with too high IL-8 concentrations (not within the linear assay range) were prediluted in a naive culture medium.

Briefly, 96-well ELISA plates (NUNC maxisorp, 442404, Thermo Fisher Scientific) were coated with the capture antibody overnight at +4 °C. The wells were aspirated and washed four times with the kit-supplied wash buffer using an automated programmable plate washer (Wallac 1296−026 Delfia Platewash, PerkinElmer Inc., Waltham, MA, USA). Nonspecific binding was blocked with assay diluent for 1 h at

RT, and wells were washed with wash buffer. Samples (100 μL) were then pipetted into the wells, and the plate was incubated for 2 h at RT. After four cycles of washes, 100 μL of detection antibody was added to each well, incubated for 1 h, and followed by four wash cycles. The avidin-HRP conjugate was added to the wells, incubated for 30 min, followed by four wash cycles. The tetramethylbenzidine substrate solution was added to each well, the plate was incubated for 15 min, and a stop solution was added to end the reaction. Optical densities were measured using a microplate reader at 450 nm wavelength and 570 nm correction wavelength. Naive culture medium served as a baseline-control sample. Samples for the standard curve were included in each assay run, and the standard curves for each assay run were generated using nonlinear regression sigmoidal 4-parameter-logistic curve-fitting. The sample concentrations were interpolated from GraphPad Prism 9 software (version 9.0.1, GraphPad Software LLC, San Diego, CA, USA). Statistical analysis was performed in GraphPad Prism using the nonparametric Mann–Whitney test with p values less than 0.05 were considered significant.

3. RESULT AND DISCUSSION

3.1. Material Compositions

Nanocellulose and chitosan, as biobased resources, demonstrate complementary properties and compatible opposing surface charges. The electrostatic interactions between these structures ensue polyionic biocomposites with excellent mechanical performance without requiring any cross-linking agent.[32] Dissolution of chitosan in mild acetic acid activates the amino groups into corresponding ammonium cations. The chitosan solutions (2 wt %) possess an effective surface charge measured by zeta potential of +42.8 mV, while the corresponding value for TEMPO-oxidized nanocellulose (TOCNF, 2 wt %) is −47 mV.

The first approach to 3D printing the mesh was directly mixing chitosan and TOCNF in an equal mass ratio and using a single printhead (Figure 1a). However, the formation of complexes upon the interaction of opposing charged polymers clogged the nozzle, subsequently (and frequently) interrupting ink extrusion. The formed complexes were noticeable after drying cast mixed gel (Figure S1). Furthermore, to examine the in situ complexation of TOCNF (2 wt %) and chitosan (2 wt %), rheological studies and wet-spinning of single coaxial filaments were performed (Figures S2 and S3).

As shown in Figure S2, the inclusion of chitosan into TOCNF aqueous suspensions profoundly impacted the rheological properties. The TOCNF Linear Viscoelastic Region (LVR) range (Figure S2a) was below 1% shear strain, and in the case of the TOCNF-chitosan mixture this range was extended up to 10% shear strain. Therefore, the mixture was a well-constituted gel with a wide linear viscoelastic response. According to these findings, all the rheology tests were performed at 0.1% shear strain within the LVR). Following the LVR test, a frequency sweep study was performed where the TOCNF-chitosan mixture exhibited an elastic modulus 1 order of magnitude higher than the analogous single-component TOCNF gel. This was due to the complexation that occurred between the two components (Figure S2b). The complexation not only affected the elastic modulus, but the viscosity and the shear stress required to overpass the inertia and triggered flow. The viscosity of the complexed material increased by 1 order of magnitude at low shear stress compared to that of the analogous TOCNF suspension, Figure S2c.

Interestingly, the mixture's viscosity decreased at high shear stresses, approaching the TOCNF suspension's viscosity values, and exhibited shear thinning behavior. In contrast,
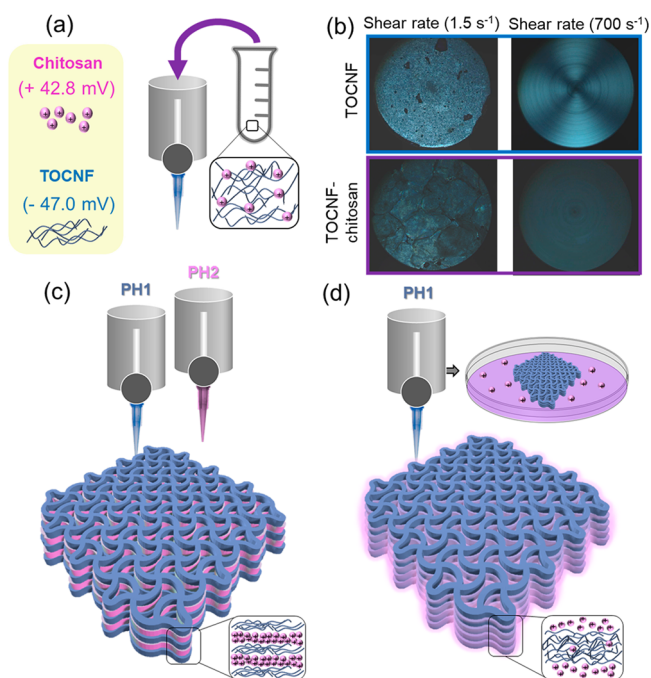

Figure 1. Schematics of the three approaches used to develop 3D printed mesh structures from nanocellulose (TOCNF) and chitosan. (a) Mixing the components before printing. (b) In situ imaging of TOCNF and TOCNF-chitosan mixture under rheology tests at low (0.15 s^{-1}) and high (700 s^{-1}) shear rates. (c) Utilization of double printheads (PH1 containing TOCNF and PH2 containing chitosan) to deposit multilayers. (d) 3D printed nanocellulose mesh followed by an immersion step in the chitosan polymer solution to obtain chitosan-sorbed nanocellulose mesh.

the minimum shear stress required to initiate flow increased from 100 kPa in TOCNF to more than 1000 kPa in the case of the complexed material (Figure S2d). In practice, this means that the pressure used for any practical flow (3D printing or spinning) must be increased more than 10-fold. The mechanical properties of the single and coaxial filaments showed complexed materials with an increased Young's modulus and tensile strength. Therefore, electrostatically complexed multilayer meshes were developed as a way to transfer the improvement of the mechanical properties observed in filaments to 3D-printed structures.

As shown in Figure 1b, pure TOCNF tended to align under high shear. At the same time, as a consequence of material complexation and despite its shear-thinning behavior, the mixture of TOCNF and chitosan did not indicate alignment, even under high shear stress. Because chitosan is soluble only in acidic pH, chitosan solutions tended to aggregate when the primary amines were deionized at pH above chitosan's pK_a (pH 6–6.5). Thus, a homogeneous mixture of TOCNF and chitosan formed within a narrow pH range and considerably low solid content, making it impractical for 3D printing. To address this challenge and ease the ink extrusion, 2 wt % TOCNF and 2 wt % chitosan were consecutively deposited via multi-printhead systems, with the layers built upon the involvement of two separate printheads (Figure 1c). TOCNF (2 wt %) formed the first layer of the mesh, considering its desirable shear-thinning rheological behavior and high printing fidelity. Thereafter, a second layer of 2 wt % chitosan was deposited on top to elicit electrostatic interactions and
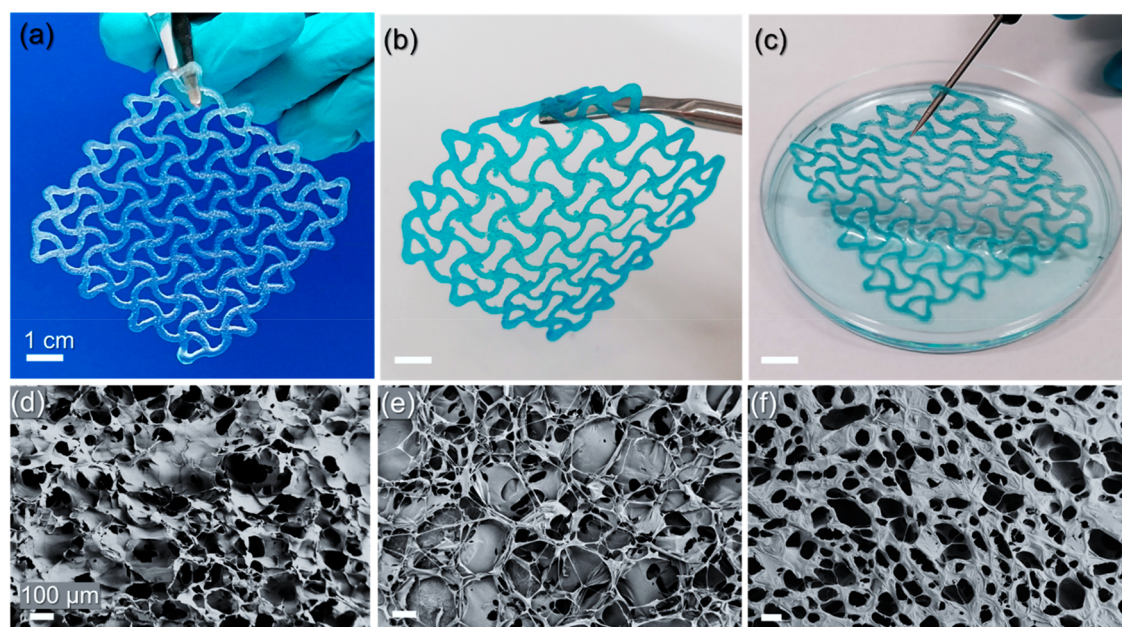
Figure 2. 3D printed mesh structures with a similar number of layers (5 layers) produced from (a) neat TOCNF, (b) TOCNF-chitosan multilayer, and (c) chitosan-sorbed TOCNF. Associated scanning electron microscope (SEM) images of the microstructures correspond to (d) neat TOCNF, (e) chitosan top layer in the TOCNF-chitosan bilayer structure (bottom layer TOCNF), and (f) chitosan-sorbed TOCNF. Scale bars: (a−c) 1 cm and (d−f) 100 μm.
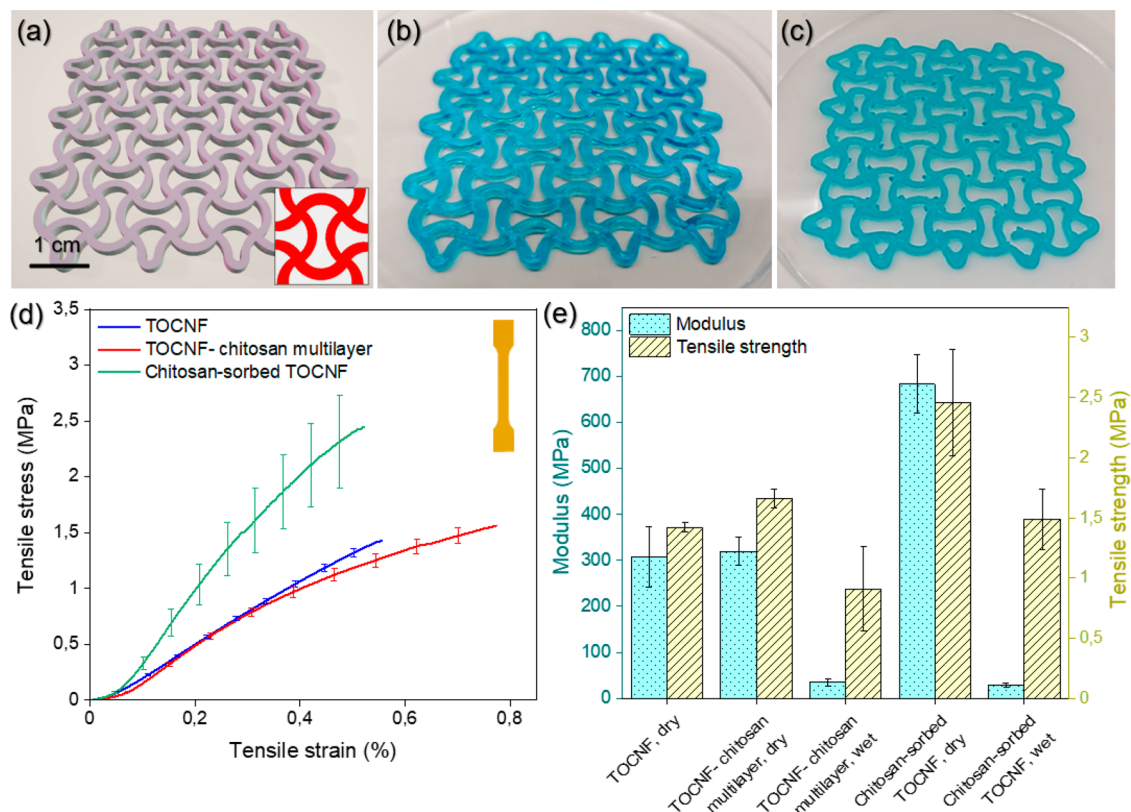

Figure 3. Shrinkage of mesh structures after immersion in ethanol. (a) Mesh 3D model used for 3D printing. Typical 3D printed mesh structure (b) before and (c) after immersion in ethanol. (d) Stress−strain profiles of 3D printed, thin, and flexible structures formed as dog bones with 100% infill and (e) comparison of he moduli and tensile strength values for the respective dry and wet structures.

complex formation, obtaining structures with high resolution and accuracy.

Our first approach to produce meshes was based on single-component TOCNF systems. Meanwhile, the main focus was on structures produced from five layers (two chitosan layers sandwiched between three layers of TOCNF). In an additional approach, the five-layered structure was entirely 3D printed from 2 wt % TOCNF, followed by a subsequent immersion in
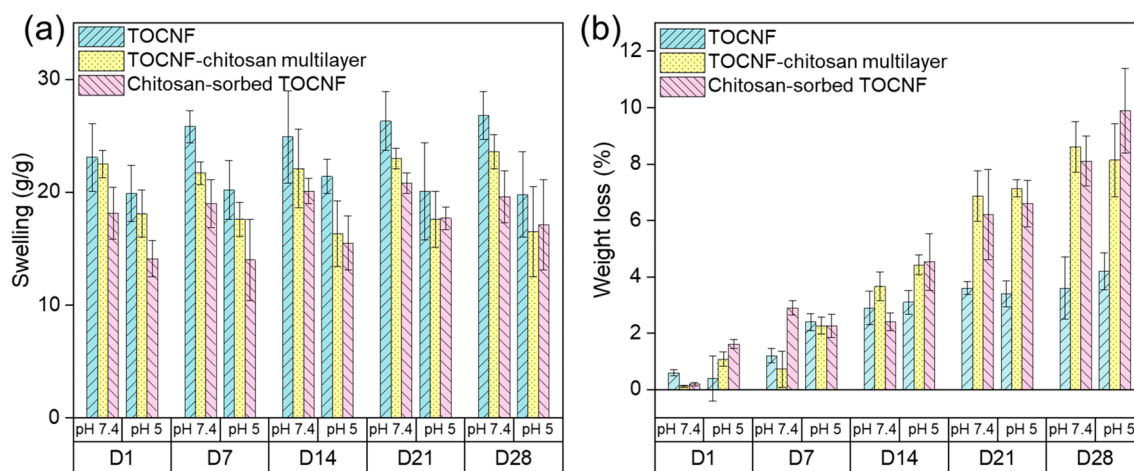
Figure 4. Swelling and weight loss of meshed prepared from neat TOCNF, TOCNF-chitosan multilayers, and chitosan-sorbed TOCNF as measured during 28 days at pH 7.4 and pH 5.

the chitosan solution. We note that the second approach facilitated complex formation at the interface between TOCNF and chitosan layers. The latter, the third approach, prompted sorption beyond the surfaces since the chitosan polymer diffused to the bulk material. The study's continuation focuses on comparing the meshed samples named as *TOCNF*, *TOCNF-chitosan multilayer* (Figure 1c), and *chitosan-sorbed TOCNF* (Figure 1d), as no material with acceptable quality was obtained from simply mixing the components.

3.2. 3D Printed Meshes Based on Nanocellulose and Chitosan

3.2.1. Microstructure.
The samples produced from the three approaches, never-dried and ethanol solvent exchange meshes of TOCNF, TOCNF-chitosan multilayer, and chitosan-sorbed TOCNF, were easy to lift, hold, and bend, showing no apparent signal of structural damage (Figure 2a–c).

Earlier studies on freeze-dried TOCNF demonstrated that the produced materials possessed a highly porous microstructure that favored nutrition and oxygen transport for the cells.[18,26] With the method presented here, the porous microstructure was retained after adding chitosan, as shown in Figure 2d–f. As confirmed by earlier studies, the nanofibrils formed on the chitosan layer (Figure 2e) were attributed to the interactions of protonated chitosan and the anionic TOCNF.[27,33] To further elucidate the chemical composition of the produced meshes, FTIR characterizations are included in Figure S4, which compares the peak position and intensity for different samples. The exhibited structures confirmed the developments of synergies between the layers.

3.2.2. Shrinkage.
About 98% of the structure in the present systems corresponded to water. The 3D printed structures underwent shrinkage upon drying due to dehydration and water removal. The shrinkage also occurred in wet conditions, via wet densification, when the geometry underwent solvent exchange or post-treatment (such as cross-linking or polymer complexation).[35] The 3D printed meshes were frozen prior to solvent exchange with ethanol to reduce the shrinkage and to retain the porous characteristics. The freezing step solidifies the structure and enhances shape and geometry retention. After immersing the samples in ethanol, ice crystals are exchanged with ethanol, which has a characteristic lower surface tension compared to water. Accordingly, wet

densification with ethanol remarkably enhances the solid volume fraction of cellulose samples.[34] We note that if the samples were immersed in ethanol, right after printing (in the absence of the freezing step), the structures would densify and the porosity of the microstructure would be reduced. For the intended applications, a porous microstructure is desirable, given its impact on the nutrition and oxygen transport required by the cells.

Herein, shrinkage of the mesh structures is reported by comparing the infill density before and after the solvent exchange with ethanol, Figure 3a–c. As mentioned earlier, the mesh structures containing smaller openings (less than 1 mm) yielded insufficient tissue integration, promoted inflammation, and enhanced bridging fibrosis.[15] Therefore, shrinkage of the 3D printed lines accounted for the increased opening size and less infill density, favoring the integration of the mesh and tissue. Image analysis with ImageJ demonstrated an overall mesh opening of 53 ± 1.2% in both 3D printed TOCNF and chitosan-TOCNF multilayer meshes. After immersion in chitosan solution, the chitosan-sorbed TOCNF exhibited a mesh opening of 61 ± 1.7% and was assigned with about 8% less infill density and larger cell openings. The chitosan-TOCNF multilayer mesh displayed about 6% larger mesh opening after three cycles of solvent exchange in ethanol.

3.2.3. Mechanical Performance.
As shown in Figure 3d and 3e, the chitosan-sorbed TOCNF demonstrated better mechanical properties (modulus and tensile strength) compared with TOCNF and TOCNF-chitosan multilayer. The electrostatic interactions of chitosan and TOCNF in the interface of the layers (TOCNF-chitosan multilayer) and bulk (chitosan-sorbed TOCNF) had a substantial effect on the mechanical properties of 3D printed full-infill dog-bone specimens. Specifically, the chitosan-sorbed TOCNF showed more than two times higher modulus and 40% higher tensile strength than those of the TOCNF-chitosan multilayer. Although the modulus of the TOCNF-chitosan multilayer and chitosan-sorbed TOCNF remained about the same in wet conditions, their tensile strength was improved considerably as the 3D printed TOCNF samples broke apart after wetting and before starting the measurement. Hydrophobic associations accompany the ionic complexation when chitosan and nanocellulose are simultaneously present in a system.[36] According to the literature, the addition of chitosan to
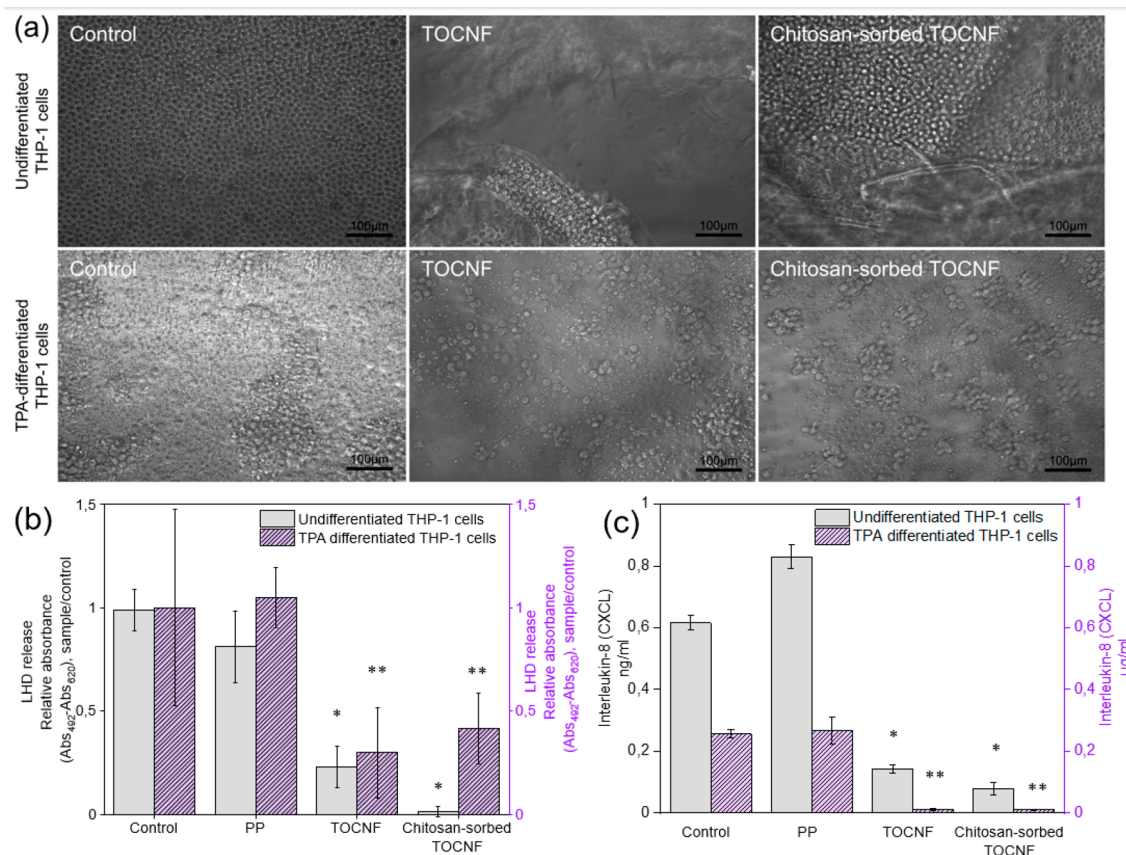
Figure 5. (a) Phase-contrast microscopy images from cultures of THP-1 cells without TPA stimulation and TPA (300 nM)-stimulated THP-1 cells for control without material, TOCNF, and chitosan-sorbed TOCNF. (b) LDH-release from a 3 day incubation of THP-1 cells with the materials, without other external cell stimulation, and with TPA (300 nM)-stimulated THP-1 cells ($*p < 0.05$, $**p < 0.01$ as compared to control). (c) Concentrations of interleukin-8 (CXCL8) in culture media after a 3 day incubation of THP-1 cells with the materials, without other external cell stimulation, and with TPA (300 nM)-stimulated THP-1 ($*p < 0.05$, $**p < 0.01$ as compared to control). Scale bars: 100 μm.

nanocellulose results in a decrease in the contact angle of the structure and the development of a denser hydrophobic nanocomposite. This occurs primarily due to the adhesion of chitosan to nanocellulose and its subsequent surface coverage. Therefore, chitosan has been reported as an additive to nanocellulose in the production of wet-strong nanopapers[37,38] and filaments.[39,40] The nanocellulose network in pure TOCNF is bond together through physical entanglement and surface interactions. Such bonds tend to dissociate upon wetting due to the reduction of hydrogen bonding. However, dehydration of chitosan/TOCNF samples enhanced the density of physical bonds and reduced the electrostatic repulsion.

3.2.4. Swelling and Weight Loss. Structural durability, translated into the extent of swelling and weight loss, is a substantial factor for biomedical implant administration. TOCNF has a high affinity to water due to the abundance of carboxyl and hydroxyl groups, and it swells extensively when placed in water. We studied the samples' swelling and weight loss at pH 7.4 (normal body condition) and pH 5 (pH associated with body areas such as the pelvis, duodenum, small intestine, and colon).[41,42] TOCNF demonstrated the highest swelling capacity, 23 ± 3 g/g, with the value reaching a plateau after about 1 day. Although the chitosan-containing samples swelled less than TOCNF did, a similar pattern was observed in achieving the maximum swelling, already after 1 day for TOCNF-chitosan multilayer and chitosan-sorbed TOCNF (Figure 4a). The maximum weight loss after 28 days was about

10% for chitosan-sorbed TOCNF (Figure 4b). Based on earlier studies, highly crystalline nanocellulose resists degradation and weight loss unless through autocatalytic oxidation, enzymatic activities, or hydrolytic processes;[43,44] such effects are not expected to occur inside the body. Therefore, we speculate that the associated minor weight loss corresponds to possible TOCNF detachment, from excess material or from handling during the experiment. In the present study, due to chitosan solubility in an acidic environment, the lower swelling and increased weight loss of chitosan-containing samples were attributed to the chitosan redissolution in a more acidic environment (pH 5).[33]

3.2.5. Cytotoxicity and Proinflammatory Cell Activation. The human monocyte cell line, THP-1, was incubated in the presence or absence of the 3D printed meshes for 3 days under cell culture conditions. Proinflammatory macrophage differentiation was induced by TPA (300 nm). Phase-contrast microscopy images of the cells are shown in Figure 5a. No dramatic differences in cell morphologies were observed, although both materials somewhat increased the size of both undifferentiated and differentiated cells. Material-induced cytotoxicity was evaluated by assessing the release of the intracellular LDH enzyme into the culture medium, reflecting cell membrane damage and activation. Both materials demonstrated a significant reduction in LDH release, suggesting good cytocompatibility with a lower rate of cell activation and membrane leakage than that of control cultures
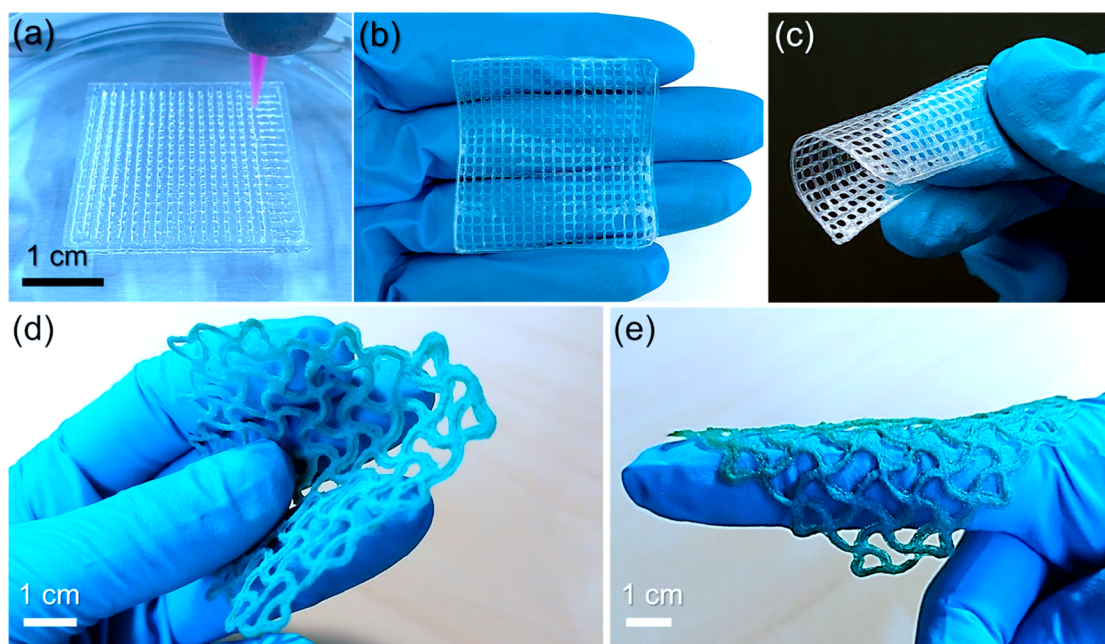
Figure 6. (a–c) Non-cross-linked freeze-dried chitosan-sorbed TOCNF. (a) 3D printed TOCNF lattice and (b, c) flexible dried chitosan-sorbed structure. (d, e) Dried chitosan-sorbed mesh structure with improved flexibility after post-treatment with glutaraldehyde. (e) Photograph of a rewet cross-linked chitosan-sorbed TOCNF.

without materials, and PP mesh (Figure 5b). Production of the proinflammatory cytokine, interleukin-8 (IL8, CXCL8), by undifferentiated monocytes and TPA-differentiated macrophages was evaluated after the 3 day incubations. Remarkably, both materials significantly suppressed the release of IL-8 from the undifferentiated cells by 4.3–7.8-fold and from the inflammatory TPA-activated macrophages by 22–24-fold (Figure 5c). Taken together with the reduction in LDH-release, this result suggests the anti-inflammatory or immunomodulatory activity of the materials deserving further attention for the increased therapeutic potential for tissue repair.

Although the developed mesh structures were solvent exchanged and maintained in ethanol (never-dried), it is possible to achieve flexible dry meshes. The chitosan-sorbed TOCNF mesh demonstrated high fidelity and flexibility, as shown in Figure 6a–c. An additional post-treatment with homobifunctional cross-linkers such as glutaraldehyde can target the primary reaction toward the amine group in chitosan to obtain mesh structures with enhanced flexibility (Figure 6d, e). Saturated dialdehydes such as glutaraldehyde have acquired wide acceptance as cross-linkers, fixators, and disinfectors in biomedicine.[45,46] Glutaraldehyde is a safe cross-linker with no cytotoxicity, provided it is utilized at a suitable concentration (below 8%).[47] Moreover, glutaraldehyde has been frequently reported as an effective cross-linker for chitosan[48,49] and nanocellulose[21,50,51] to form mechanically robust structures, forming irreversible covalent bonds between macromolecular chains. Although the cross-linking post-treatment was optional, it is critical to select a suitable cross-linking approach. For instance, the commonly reported aqueous salt immersion (CaCl$_2$, 1M) cross-linking produced more brittle structures (Figure S5).

Overall, DIW is a promising technique for developing customized structures and fine-tuning the properties according to the desired applications. The excellent biocompatibility and negligible cytotoxicity toward human monocyte/macrophages make the nanocellulose/chitosan compositions (meshes) great options for further in vivo investigations.

4. CONCLUSIONS

This study examined possible approaches to process chitosan and nanocellulose by Direct Ink Writing (DIW) to develop mesh implants. The DIW technique is shown as a promising approach to adjust all the required geometrical details such as mesh shape, dimensions, infill density, and opening size. The investigated approaches included mixing the biomaterial, layer-by-layer deposition of oppositely charged components via multiple printheads, and chitosan-sorbed post-treatment on 3D printed nanocellulose meshes. The chitosan-sorbed nanocellulose displayed the best performance within all samples, with a modulus as high as 683 ± 63 MPa and tensile strength of 2.46 ± 0.44 MPa, while the associated values for pure nanocellulose were 307 and 0.25 MPa, respectively. The samples exhibited a maximum of 10% weight loss after 28 days of immersion in pH 7.4 and 5. The biological observations showed excellent biocompatibility, negligible cytotoxicity, and pro-inflammatory activation-suppressing activity for chitosan-sorbed TOCNF in THP-1 human monocyte/macrophages, indicating these biocomposites as a promising candidate for implant administration.

■ ASSOCIATED CONTENT

ⓢ Supporting Information

The Supporting Information is available free of charge at https://pubs.acs.org/doi/10.1021/acspolymersau.1c00045.

Image of a film cast from TOCNF and chitosan and the formed complexes clogging the nozzle during the 3D printing process; rheological properties of TOCNF 2 wt %, chitosan 2 wt %, and their mixture using an equal mass ratio (linear viscoelastic region, frequency sweep, solution viscosities at different shear rates, and flow yield

strain test); mechanical properties of a single TOCNF filament and its comparison with a composed filament (core and shell) with an outer layer of TOCNF 2 wt % and the inner layer of Ch 2 wt %; chemical characterization of TOCNF, chitosan, TCNF-chitosan multilayer, and chitosan-sorbed TOCNF; mesh cross-linked in CaCl₂ (1 M, 10 min immersion) obtained a highly brittle structure that breaks when bent (PDF)

■ AUTHOR INFORMATION

Corresponding Author

Orlando J. Rojas − *Department of Bioproducts and Biosystems, School of Chemical Engineering, Aalto University, FI-00076 Aalto, Espoo, Finland; Bioproducts Institute, Department of Chemical & Biological Engineering, Department of Chemistry and Department of Wood Science, 2360 East Mall, The University of British Columbia, Vancouver, BC V6T 1Z3, Canada;* ⊙ orcid.org/0000-0003-4036-4020; Phone: +1-604-822-3457; Email: orlando.rojas@aalto.fi

Authors

Rubina Ajdary − *Department of Bioproducts and Biosystems, School of Chemical Engineering, Aalto University, FI-00076 Aalto, Espoo, Finland; Bioproducts Institute, Department of Chemical & Biological Engineering, Department of Chemistry and Department of Wood Science, 2360 East Mall, The University of British Columbia, Vancouver, BC V6T 1Z3, Canada*

Guillermo Reyes − *Department of Bioproducts and Biosystems, School of Chemical Engineering, Aalto University, FI-00076 Aalto, Espoo, Finland;* ⊙ orcid.org/0000-0002-3468-1137

Jani Kuula − *Department of Neuroscience and Biomedical Engineering, School of Science, Aalto University, FI-00076 Aalto, Espoo, Finland*

Eija Raussi-Lehto − *Department of Neuroscience and Biomedical Engineering, School of Science, Aalto University, FI-00076 Aalto, Espoo, Finland; R&D Development Services, Metropolia University of Applied Sciences, FI-00079 Metropolia, Helsinki, Finland*

Tomi S. Mikkola − *Department of Obstetrics and Gynecology, University of Helsinki, and Helsinki University Hospital, 00290 Helsinki, Finland*

Esko Kankuri − *Department of Pharmacology, Faculty of Medicine, University of Helsinki, 00290 Helsinki, Finland;* ⊙ orcid.org/0000-0002-2193-8773

Complete contact information is available at:
https://pubs.acs.org/10.1021/acspolymersau.1c00045

Author Contributions

The manuscript was written through the contributions of all authors. All authors have given approval to the final version of the manuscript.

Notes

The authors declare no competing financial interest.

■ REFERENCES

(1) Knight, K. M.; Moalli, P. A.; Abramowitch, S. D. Preventing Mesh Pore Collapse by Designing Mesh Pores with Auxetic Geometries: A Comprehensive Evaluation Via Computational Modeling. *J. Biomech. Eng.* **2018**, *140* (5), 1−8.

(2) Barone, W. R.; Moalli, P. A.; Abramowitch, S. D. Textile Properties of Synthetic Prolapse Mesh in Response to Uniaxial Loading. *Am. J. Obstet. Gynecol* **2016**, *215* (3), 326.e1−326.e9.

(3) Mangir, N.; Aldemir Dikici, B.; Chapple, C. R.; MacNeil, S. Landmarks in Vaginal Mesh Development: Polypropylene Mesh for Treatment of SUI and POP. *Nat. Rev. Urol.* **2019**, *16* (11), 675−689.

(4) Iakovlev, V. V.; Guelcher, S. A.; Bendavid, R. Degradation of Polypropylene in Vivo: A Microscopic Analysis of Meshes Explanted from Patients. *J. Biomed. Mater. Res., Part B* **2017**, *105B* (2), 237−248.

(5) U.S. Food & Drug Administration. *FDA takes action to protect women's health, orders manufacturers of surgical mesh intended for transvaginal repair of pelvic organ prolapse to stop selling all devices.* https://www.fda.gov/news-events/press-announcements/fda-takes-action-protect-womens-health-orders-manufacturers-surgical-mesh-intended-transvaginal (accessed July 2021).

(6) Li, T.; Chen, C.; Brozena, A. H.; Zhu, J. Y.; Xu, L.; Driemeier, C.; Dai, J.; Rojas, O. J.; Isogai, A.; Wågberg, L.; Hu, L. Developing Fibrillated Cellulose as a Sustainable Technological Material. *Nature* **2021**, *590* (7844), 47−56.

(7) Curvello, R.; Raghuwanshi, V. S.; Garnier, G. Engineering Nanocellulose Hydrogels for Biomedical Applications. *Adv. Colloid Interface Sci.* **2019**, *267*, 47−61.

(8) Ajdary, R.; Tardy, B. L.; Mattos, B. D.; Bai, L.; Rojas, O. J. Plant Nanomaterials and Inspiration from Nature: Water Interactions and Hierarchically Structured Hydrogels. *Adv. Mater.* **2021**, *33*, 2001085.

(9) Lundahl, M. J.; Klar, V.; Ajdary, R.; Norberg, N.; Ago, M.; Cunha, A. G.; Rojas, O. J. Absorbent Filaments from Cellulose Nanofibril Hydrogels through Continuous Coaxial Wet Spinning. *ACS Appl. Mater. Interfaces* **2018**, *10* (32), 27287−27296.

(10) Hsieh, Y. Lo Cellulose Nanofibers: Electrospinning and Nanocellulose Self-Assemblies. *In Advanced Green Composites; Scrivener Publishing LLC 67* **2018**, 67−95.

(11) Baniasadi, H.; Ajdary, R.; Trifol, J.; Rojas, O. J.; Seppala, J. Direct Ink Writing of Aloe Vera/Cellulose Nanofibrils Bio-Hydrogels. *Carbohydr. Polym.* **2021**, *266* (April), 118114.

(12) Intini, C.; Elviri, L.; Cabral, J.; Mros, S.; Bergonzi, C.; Bianchera, A.; Flammini, L.; Govoni, P.; Barocelli, E.; Bettini, R.; McConnell, M. 3D-Printed Chitosan-Based Scaffolds: An in Vitro Study of Human Skin Cell Growth and an in-Vivo Wound Healing Evaluation in Experimental Diabetes in Rats. *Carbohydr. Polym.* **2018**, *199*, 593−602.

(13) Peter, S.; Lyczko, N.; Gopakumar, D.; Maria, H. J.; Nzihou, A.; Thomas, S. Chitin and Chitosan Based Composites for Energy and Environmental Applications: A Review. *Waste Biomass Valorization* **2021**, *12*, 4777−4804.

(14) Zhou, L.; Ramezani, H.; Sun, M.; Xie, M.; Nie, J.; Lv, S.; Cai, J.; Fu, J.; He, Y. 3D Printing of High-Strength Chitosan Hydrogel Scaffolds without Any Organic Solvents. *Biomater. Sci.* **2020**, *8* (18), 5020−5028.

(15) Orenstein, S. B.; Saberski, E. R.; Kreutzer, D. L.; Novitsky, Y. W. Comparative Analysis of Histopathologic Effects of Synthetic Meshes Based on Material, Weight, and Pore Size in Mice. *J. Surg. Res.* **2012**, *176* (2), 423−429.

(16) Schmidt, A.; Taylor, D. Erosion of Soft Tissue by Polypropylene Mesh Products. *J. Mech. Behav. Biomed. Mater.* **2021**, *115*, 104281.

(17) Olmos-Juste, R.; Alonso-Lerma, B.; Pérez-Jiménez, R.; Gabilondo, N.; Eceiza, A. 3D Printed Alginate-Cellulose Nanofibers Based Patches for Local Curcumin Administration. *Carbohydr. Polym.* **2021**, *264* (July), 118026.

(18) Ajdary, R.; Ezazi, N. Z.; Correia, A.; Kemell, M.; Huan, S.; Ruskoaho, H. J.; Hirvonen, J.; Santos, H. A.; Rojas, O. J. Multifunctional 3D-Printed Patches for Long-Term Drug Release Therapies after Myocardial Infarction. *Adv. Funct. Mater.* **2020**, *30* (34), 2003440.

(19) Kean, T. J.; Thanou, M. Utility of Chitosan for 3D Printing and Bioprinting. *In Sustainable Agriculture Reviews* **2019**, *35*, 271−292.

(20) Kamdem Tamo, A.; Doench, I.; Walter, L.; Montembault, A.; Sudre, G.; David, L.; Morales-Helguera, A.; Selig, M.; Rolauffs, B.; Bernstein, A.; Hoenders, D.; Walther, A.; Osorio-Madrazo, A. Development of Bioinspired Functional Chitosan/Cellulose Nano-fiber 3d Hydrogel Constructs by 3d Printing for Application in the Engineering of Mechanically Demanding Tissues. *Polymers (Basel).* **2021**, *13*, 1663.

(21) Sampath, U. G. T. M.; Ching, Y. C.; Chuah, C. H.; Singh, R.; Lin, P. C. Preparation and Characterization of Nanocellulose Reinforced Semi-Interpenetrating Polymer Network of Chitosan Hydrogel. *Cellulose* **2017**, *24*, 2215−2228.

(22) Hänninen, A.; Sarlin, E.; Lyyra, I.; Salpavaara, T.; Kellomäki, M.; Tuukkanen, S. Nanocellulose and Chitosan Based Films as Low Cost, Green Piezoelectric Materials. *Carbohydr. Polym.* **2018**, *202*, 418−424.

(23) Cleymand, F.; Poerio, A.; Mamanov, A.; Elkhoury, K.; Ikhelf, L.; Jehl, J. P.; Kahn, C. J. F.; Ponçot, M.; Arab-Tehrany, E.; Mano, J. F. Development of Novel Chitosan/Guar Gum Inks for Extrusion-Based 3D Bioprinting: Process, Printability and Properties. *Bioprinting* **2021**, *21* (March), No. e00122.

(24) Zhao, Y. F.; Zhao, J. Y.; Hu, W. Z.; Ma, K.; Chao, Y.; Sun, P. J.; Fu, X. B.; Zhang, H. Synthetic Poly(Vinyl Alcohol)-Chitosan as a New Type of Highly Efficient Hemostatic Sponge with Blood-Triggered Swelling and High Biocompatibility. *J. Mater. Chem. B* **2019**, *7* (11), 1855−1866.

(25) Venkatesan, J.; Kim, S. K. Chitosan Composites for Bone Tissue Engineering - An Overview. *Mar. Drugs* **2010**, *8* (8), 2252−2266.

(26) Ajdary, R.; Huan, S.; Zanjanizadeh Ezazi, N.; Xiang, W.; Grande, R.; Santos, H. A. H. A.; Rojas, O. J. O. J. Acetylated Nanocellulose for Single-Component Bioinks and Cell Proliferation on 3D-Printed Scaffolds. *Biomacromolecules* **2019**, *20* (7), 2770−2778.

(27) Grande, R.; Trovatti, E.; Carvalho, A. J. F.; Gandini, A. Continuous Microfiber Drawing by Interfacial Charge Complexation between Anionic Cellulose Nanofibers and Cationic Chitosan. *J. Mater. Chem. A* **2017**, *5* (25), 13098−13103.

(28) Jeon, J. G.; Kim, H. C.; Palem, R. R.; Kim, J.; Kang, T. J. Cross-Linking of Cellulose Nanofiber Films with Glutaraldehyde for Improved Mechanical Properties. *Mater. Lett.* **2019**, *250*, 99−102.

(29) Rueden, C. T.; Schindelin, J.; Hiner, M. C.; DeZonia, B. E.; Walter, A. E.; Arena, E. T.; Eliceiri, K. W. ImageJ2: ImageJ for the next Generation of Scientific Image Data. *BMC Bioinf.* **2017**, *18* (1), 529.

(30) Väänänen, A. J.; Salmenperä, P.; Hukkanen, M.; Rauhala, P.; Kankuri, E. Cathepsin B Is a Differentiation-Resistant Target for Nitroxyl (HNO) in THP-1 Monocyte/Macrophages. *Free Radical Biol. Med.* **2006**, *41* (1), 120−131.

(31) Den Hollander, B.; Sundström, M.; Pelander, A.; Siltanen, A.; Ojanperä, I.; Mervaala, E.; Korpi, E. R.; Kankuri, E. Mitochondrial Respiratory Dysfunction Due to the Conversion of Substituted Cathinones to Methylbenzamides in SH-SY5Y Cells. *Sci. Rep.* **2015**, *5* (5), 14294.

(32) Facchine, E. G.; Bai, L.; Rojas, O. J.; Khan, S. A. Associative Structures Formed from Cellulose Nanofibrils and Nanochitins Are

PH-Responsive and Exhibit Tunable Rheology. *J. Colloid Interface Sci.* **2021**, *588*, 232−241.

(33) Toivonen, M. S.; Kurki-Suonio, S.; Wagermaier, W.; Hynninen, V.; Hietala, S.; Ikkala, O. Interfacial Polyelectrolyte Complex Spinning of Cellulose Nanofibrils for Advanced Bicomponent Fibers. *Biomacromolecules* **2017**, *18* (4), 1293−1301.

(34) Hausmann, M. K.; Siqueira, G.; Libanori, R.; Kokkinis, D.; Neels, A.; Zimmermann, T.; Studart, A. R. Complex-Shaped Cellulose Composites Made by Wet Densification of 3D Printed Scaffolds. *Adv. Funct. Mater.* **2020**, *30* (4), 1904127.

(35) Hausmann, M. K.; Siqueira, G.; Libanori, R.; Kokkinis, D.; Neels, A.; Zimmermann, T.; Studart, A. R. Complex-Shaped Cellulose Composites Made by Wet Densification of 3D Printed Scaffolds. *Adv. Funct. Mater.* **2020**, *30* (4), 1904127.

(36) Szymańska-Chargot, M.; Chylińska, M.; Pertile, G.; Pieczywek, P. M.; Cieślak, K. J.; Zdunek, A.; Frąc, M. Influence of Chitosan Addition on the Mechanical and Antibacterial Properties of Carrot Cellulose Nanofibre Film. *Cellulose* **2019**, *26*, 9613−9629.

(37) Toivonen, M. S.; Kurki-Suonio, S.; Schacher, F. H.; Hietala, S.; Rojas, O. J.; Ikkala, O. Water-Resistant, Transparent Hybrid Nanopaper by Physical Cross-Linking with Chitosan. *Biomacromolecules* **2015**, *16* (3), 1062−1071.

(38) Gao, Q.; Lei, M.; Zhou, K.; Liu, X.; Wang, S.; Li, H. Preparation of a Microfibrillated Cellulose/Chitosan/Polypyrrole Film for Active Food Packaging. *Prog. Org. Coatings* **2020**, *149*, 105907.

(39) Cai, Y.; Geng, L.; Chen, S.; Shi, S.; Hsiao, B. S.; Peng, X. Hierarchical Assembly of Nanocellulose into Filaments by Flow-Assisted Alignment and Interfacial Complexation: Conquering the Conflicts between Strength and Toughness. *ACS Appl. Mater. Interfaces* **2020**, *12* (28), 32090−32098.

(40) Zhang, K.; Ketterle, L.; Järvinen, T.; Hong, S.; Liimatainen, H. Conductive Hybrid Filaments of Carbon Nanotubes, Chitin Nano-crystals and Cellulose Nanofibers Formed by Interfacial Nanoparticle Complexation. *Mater. Des.* **2020**, *191*, 108594.

(41) Fallingborg, J. Intraluminal PH of the Human Gastrointestinal Tract. *Dan. Med. Bull.* **1999**, *43* (6), 183−196.

(42) Savchenko, M. Normal Vaginal pH: How to Test, Balance, and Restore Vaginal pH. *Flo Health, Inc.* https://flo.health/menstrual-cycle/health/symptoms-and-diseases/normal-vaginal-ph-balance (accessed July 2021).

(43) Łojewska, J.; Miśkowiec, P.; Łojewski, T.; Proniewicz, L. M. Cellulose Oxidative and Hydrolytic Degradation: In Situ FTIR Approach. *Polym. Degrad. Stab.* **2005**, *88* (3), 512−520.

(44) Lin, N.; Dufresne, A. Nanocellulose in Biomedicine: Current Status and Future Prospect. *Eur. Polym. J.* **2014**, *59*, 302−325.

(45) Lin, W.; Yuan, D.; Deng, Z.; Niu, B.; Chen, Q. The Cellular and Molecular Mechanism of Glutaraldehyde-Didecyldimethylammo-nium Bromide as a Disinfectant against Candida Albicans. *J. Appl. Microbiol.* **2019**, *126*, 102−112.

(46) Jayakrishnan, A.; Jameela, S. R. Glutaraldehyde as a Fixative in Bioprostheses and Drug Delivery Matrices. *Biomaterials* **1996**, *17* (5), 471−484.

(47) Reddy, N.; Reddy, R.; Jiang, Q. Crosslinking Biopolymers for Biomedical Applications. *Trends Biotechnol.* **2015**, *33* (6), 362−369.

(48) Beppu, M. M.; Vieira, R. S.; Aimoli, C. G.; Santana, C. C. Crosslinking of Chitosan Membranes Using Glutaraldehyde: Effect on Ion Permeability and Water Absorption. *J. Membr. Sci.* **2007**, *301* (1−2), 126−130.

(49) Monteiro, O. A.C; Airoldi, C. Some Studies of Crosslinking Chitosan-Glutaraldehyde Interaction in a Homogeneous System. *Int. J. Biol. Macromol.* **1999**, *26* (2−3), 119−128.

(50) Hanif, Z.; Choi, D.; Tariq, M. Z.; La, M.; Park, S. J. Water-Stable Flexible Nanocellulose Chiral Nematic Films through Acid Vapor Cross-Linked Glutaraldehyde for Chiral Nematic Templating. *ACS Macro Lett.* **2020**, *9* (2), 146−151.

(51) Chen, Y.; Zhang, L.; Yang, Y.; Pang, B.; Xu, W.; Duan, G.; Jiang, S.; Zhang, K. Recent Progress on Nanocellulose Aerogels:

Preparation, Modification, Composite Fabrication, Applications. *Adv. Mater.* **2021**, *33*, 2005569.